

Supporting Information

The Impact of the Bulk Structure on Surface Dynamics of Complex Mo-V-based Oxide Catalysts

Annette Trunschke,^{1,*} Johannes Noack,^{1,2} Sergej Trojanov,³ Frank Girgsdies,¹
Thomas Lunkenbein,¹ Verena Pfeifer,^{1,4} Michael Hävecker,^{1,5} Pierre Kube,¹
Christoph Sprung,¹ Frank Rosowski,⁶ Robert Schlögl¹

¹Department of Inorganic Chemistry, Fritz-Haber-Institut der Max-Planck-Gesellschaft,
Faradayweg 4-6, 14195, Berlin, Germany

²UniCat-BASF Joint Lab, Technische Universität Berlin, Sekr. EW K 01, Hardenbergstraße
36, 10623 Berlin, Germany

³Humboldt-Universität zu Berlin, Institut für Chemie, Brook-Taylor-Str. 2, 12489 Berlin,
Germany

⁴Catalysis for Energy, Group EM-GKAT, Helmholtz-Zentrum Berlin für Materialien und
Energie GmbH, Elektronenspeicherring BESSY II, Albert-Einstein-Str. 15, 12489 Berlin,
Germany

⁵Department of Heterogeneous Reactions, Max-Planck-Institut für Chemische
Energiekonversion, Stiftstr. 34-36, 45470 Mülheim a. d. Ruhr, Germany

⁶BASF SE, Process Research and Chemical Engineering, Heterogeneous Catalysis, Carl-
Bosch-Straße 38, 67056, Ludwigshafen, Germany

Corresponding author: trunschke@fhi-berlin.mpg.de

Table S1. Atomic coordinates and (equivalent) isotropic displacement parameters ($\text{\AA}^2 \times 10^3$) for MoVO_x . U_{eq} is defined as one third of the trace of the orthogonalized U_{ij} tensor

	x	y	Z	Occupancy	$U_{\text{eq}} / U_{\text{iso}}$
Mo/V(1)	0.5	0.5	0.4123(9)	0.26(2) / 0.74(2)	9(1)
Mo(2)	-0.0049(1)	0.5083(1)	0.5488(9)	0.5	15(1)
Mo/V(3)	0.1170(1)	0.2308(1)	0.4049(6)	0.242(17) / 0.758(17)	9(1)
Mo/V(4)	0.1772(1)	0.4778(1)	0.4329(7)	0.552(18) / 0.448(18)	25(1)
Mo(5)	0.2099(1)	0.3438(1)	0.5727(4)	1	8(1)
Mo(6)	0.2821(1)	0.2112(1)	0.5687(4)	1	6(1)
Mo/V(7)	0.3848(1)	0.1029(1)	0.4210(7)	0.454(18) / 0.546(18)	22(1)
Mo(8)	0.4585(1)	0.2256(1)	0.5734(5)	1	9(1)
Mo(9)	0.3592(1)	0.3184(1)	0.4112(4)	1	6(1)
Mo(10)	0.5012(1)	0.3659(1)	0.5718(4)	1	4(1)
Mo(11)	0.3443(1)	0.4409(1)	0.5629(4)	1	7(1)
V(12)	0.0611(6)	0.4021(5)	0.4940(30)	0.243(9)	15(3)
V(121)	0.0379(6)	0.3954(5)	0.4920(30)	0.243(9)	15(3)
O(1)	0.5	0.5	0.0020(30)	1	9(3)
O(2)	0	0.5	0.0000(40)	1	21(4)
O(3)	0.1179(6)	0.2306(5)	-0.0020(30)	1	21(3)
O(4)	0.1770(5)	0.4760(4)	0.0000(30)	1	18(3)
O(5)	0.2150(5)	0.3444(4)	0.0090(30)	1	14(2)
O(6)	0.2847(5)	0.2155(4)	0.0040(30)	1	18(3)
O(7)	0.3856(5)	0.1035(5)	-0.0030(30)	1	19(3)
O(8)	0.4546(6)	0.2284(5)	0.0120(40)	1	27(3)
O(9)	0.3590(4)	0.3187(3)	-0.0120(20)	1	4(2)
O(10)	0.4953(5)	0.3635(4)	0.0080(30)	1	9(2)
O(11)	0.3430(4)	0.4371(4)	0.0000(20)	1	7(2)
O(12)	0.0580(20)	0.3777(19)	0.9850(130)	0.26(4)	20
O(121)	0.0590(20)	0.3667(17)	0.1820(140)	0.28(4)	20
O(13)	0.5209(4)	0.4306(4)	0.4970(20)	1	5(2)
O(14)	0.5743(4)	0.3325(4)	0.4940(20)	1	4(2)
O(15)	0.5388(5)	0.2336(4)	0.4910(20)	1	9(2)
O(16)	0.0828(5)	0.4701(4)	0.4860(20)	1	11(2)
O(17)	0.1991(5)	0.2029(4)	0.4940(20)	1	9(2)
O(18)	0.2745(4)	0.2880(3)	0.4910(20)	1	0(2)
O(19)	0.1735(5)	0.4036(4)	0.4930(30)	1	13(2)
O(20)	0.0370(5)	0.5643(4)	0.4870(30)	1	15(2)
O(21)	0.3157(4)	0.1492(4)	0.4900(20)	1	4(2)
O(22)	0.2971(4)	0.3740(3)	0.4860(20)	1	1(2)
O(23)	0.2688(4)	0.4744(3)	0.4890(20)	1	5(2)
O(24)	0.3673(4)	0.2439(4)	0.4800(20)	1	5(2)
O(25)	0.4064(4)	0.3829(3)	0.4830(20)	1	2(2)
O(26)	0.4078(5)	0.4838(4)	0.4920(20)	1	11(2)
O(27)	0.1671(5)	0.5461(4)	0.4800(20)	1	10(2)
O(28)	0.4424(5)	0.1603(4)	0.4960(30)	1	13(2)
O(29)	0.4492(4)	0.3013(3)	0.4880(20)	1	1(2)
O(30)	0.1515(4)	0.2977(4)	0.4970(20)	1	6(2)
O(31)	0.1780(20)	0.0874(19)	0.4900(110)	0.25(3)	20
O(32)	0.1837(12)	0.0857(10)	0.0000(60)	0.46(3)	20

Table S2. Anisotropic displacement parameters ($\text{\AA}^2 \times 10^3$) for MoVO_x. The anisotropic displacement factor exponent takes the form: $-2\pi^2|\mathbf{h}^2 \mathbf{a}^{*2} U_{11} + \dots + 2 \mathbf{h} \cdot \mathbf{k} \mathbf{a}^* \mathbf{b}^* U_{12}|$

	U_{11}	U_{22}	U_{33}	U_{23}	U_{13}	U_{12}
M(1)	7(1)	7(1)	13(2)	0	0	-1(1)
M(3)	4(1)	11(1)	12(1)	-1(1)	1(1)	-2(1)
M(4)	11(1)	11(1)	53(2)	2(1)	0(1)	4(1)
Mo(5)	4(1)	8(1)	11(1)	0(1)	0(1)	0(1)
Mo(6)	4(1)	9(1)	6(1)	0(1)	0(1)	0(1)
M(7)	15(1)	9(1)	42(1)	-2(1)	-1(1)	1(1)
Mo(8)	5(1)	10(1)	14(1)	1(1)	-1(1)	0(1)
Mo(9)	3(1)	6(1)	8(1)	-1(1)	0(1)	0(1)
Mo(10)	4(1)	6(1)	3(1)	0(1)	0(1)	0(1)
Mo(11)	4(1)	9(1)	7(1)	-1(1)	0(1)	-1(1)

Table S3. V 2p_{3/2} fit parameters (Fig. 10 in the main text)

Species	V 2p _{3/2} 4+	V 2p _{3/2} 5+ (I)	V 2p _{3/2} 5+ (II)
Fwhm	1.4-1.45	1.25-1.35	1.25-1.35
Position	516.1	517.1	517.3
line shape	GL(40)	GL(40)	GL(40)

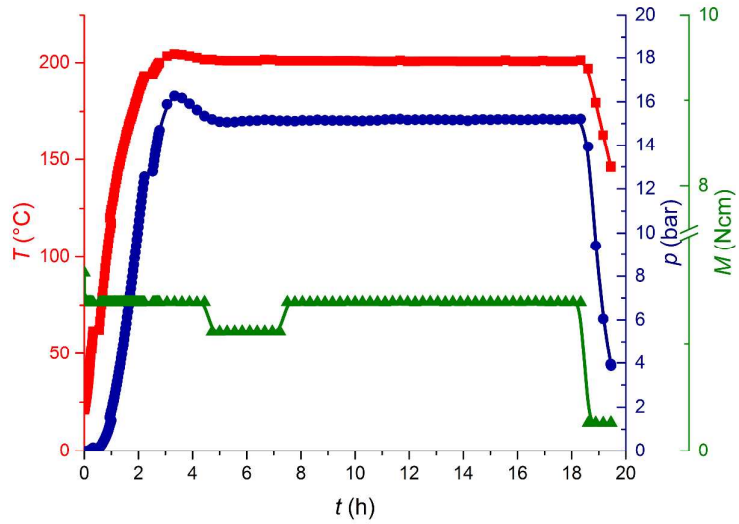


Figure S1. Relative pressure (blue), force applied by the stirrer (green), and temperature profile (red) within the autoclave during hydrothermal synthesis. The relative pressure is defined as the difference between the pressure inside the autoclave minus the atmospheric pressure.

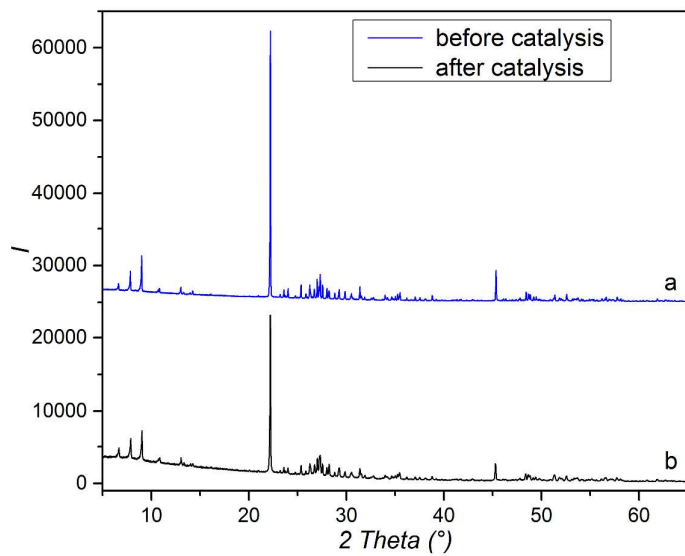


Figure S2. PXRD of fresh $(\text{Mo},\text{V})\text{O}_x$ (ID 18075) (a), lattice constants $a=21.0426(2)$ Å, $b=26.5017(4)$ Å, $c=3.99508(3)$ Å, and of the catalyst used in oxidative dehydrogenation of propane and ethane at 250–300°C (ID 24985) (b), lattice constants $a=21.0637(4)$ Å, $b=26.5075(7)$ Å, $c=4.00219(7)$ Å.

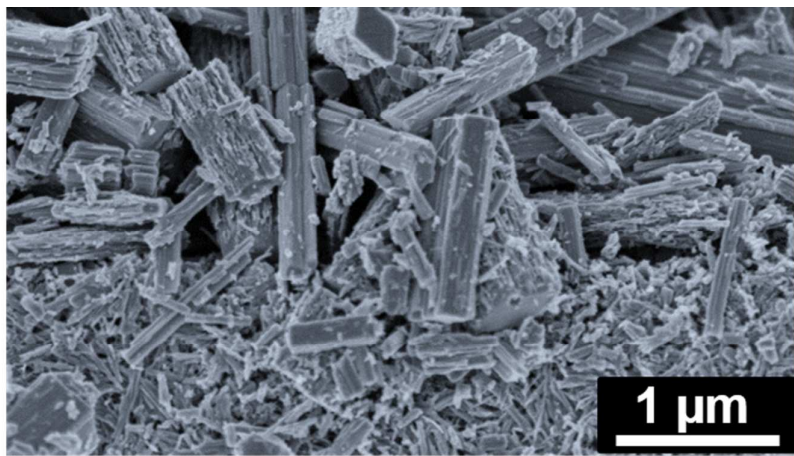


Figure S3. SEM image of $(\text{Mo},\text{V})\text{O}_x$.

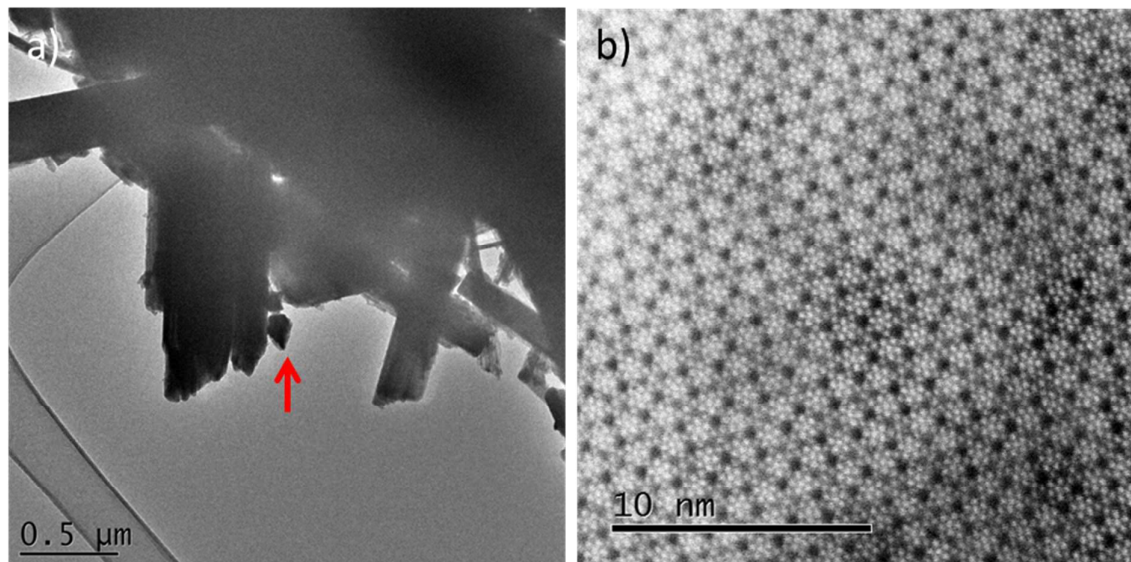


Figure S4. Exemplified high-resolution TEM image (right) of one small $(\text{Mo},\text{V})\text{O}_x$ particle selected by transmission electron microscopy (left, particle indicated by the red arrow).

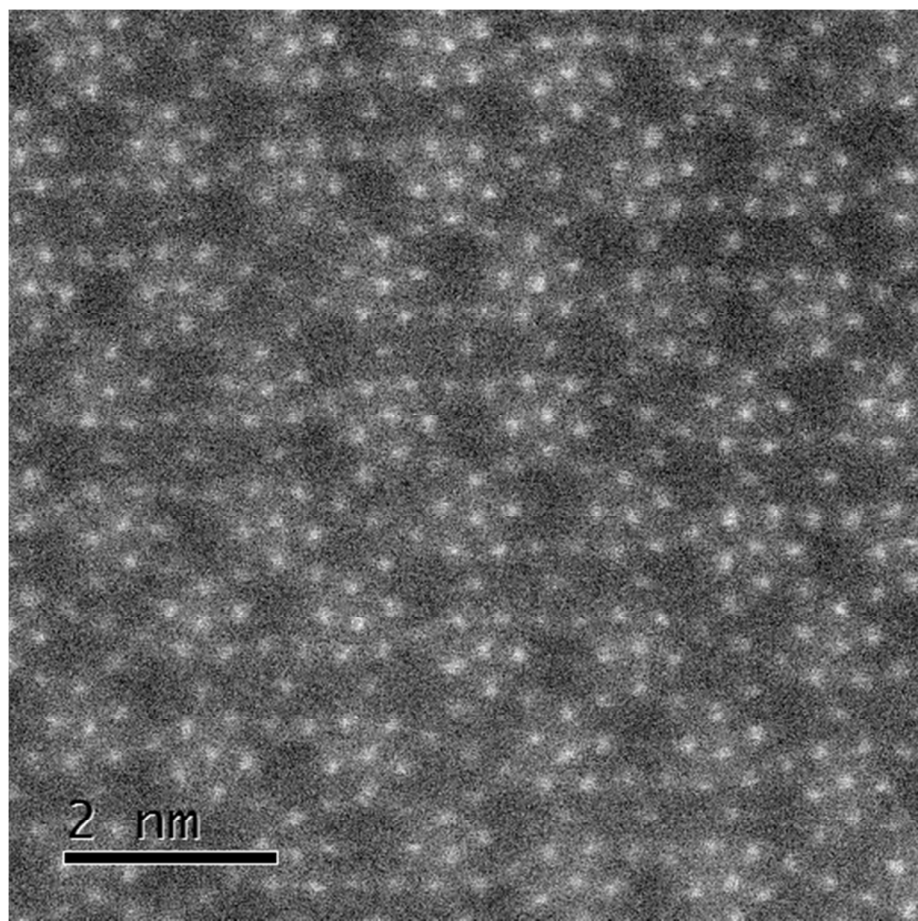


Figure S5. Atomic resolution HAADF-STEM image of $(\text{Mo},\text{V})\text{O}_x$ viewed along [001].

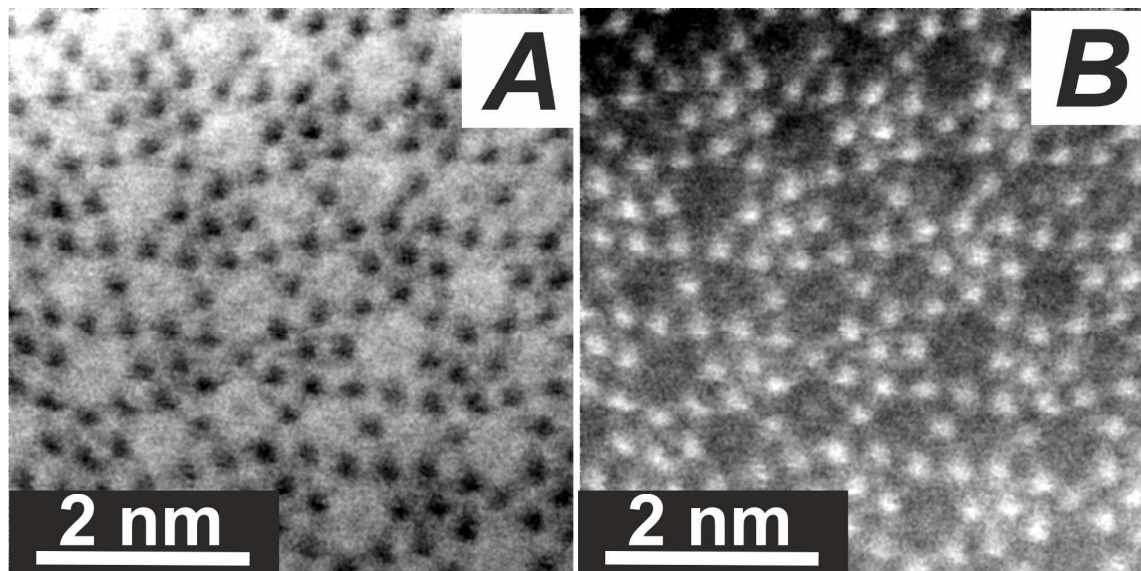


Figure S6. Uncoloured ABF-STEM images (A) regular and (B) inverted.

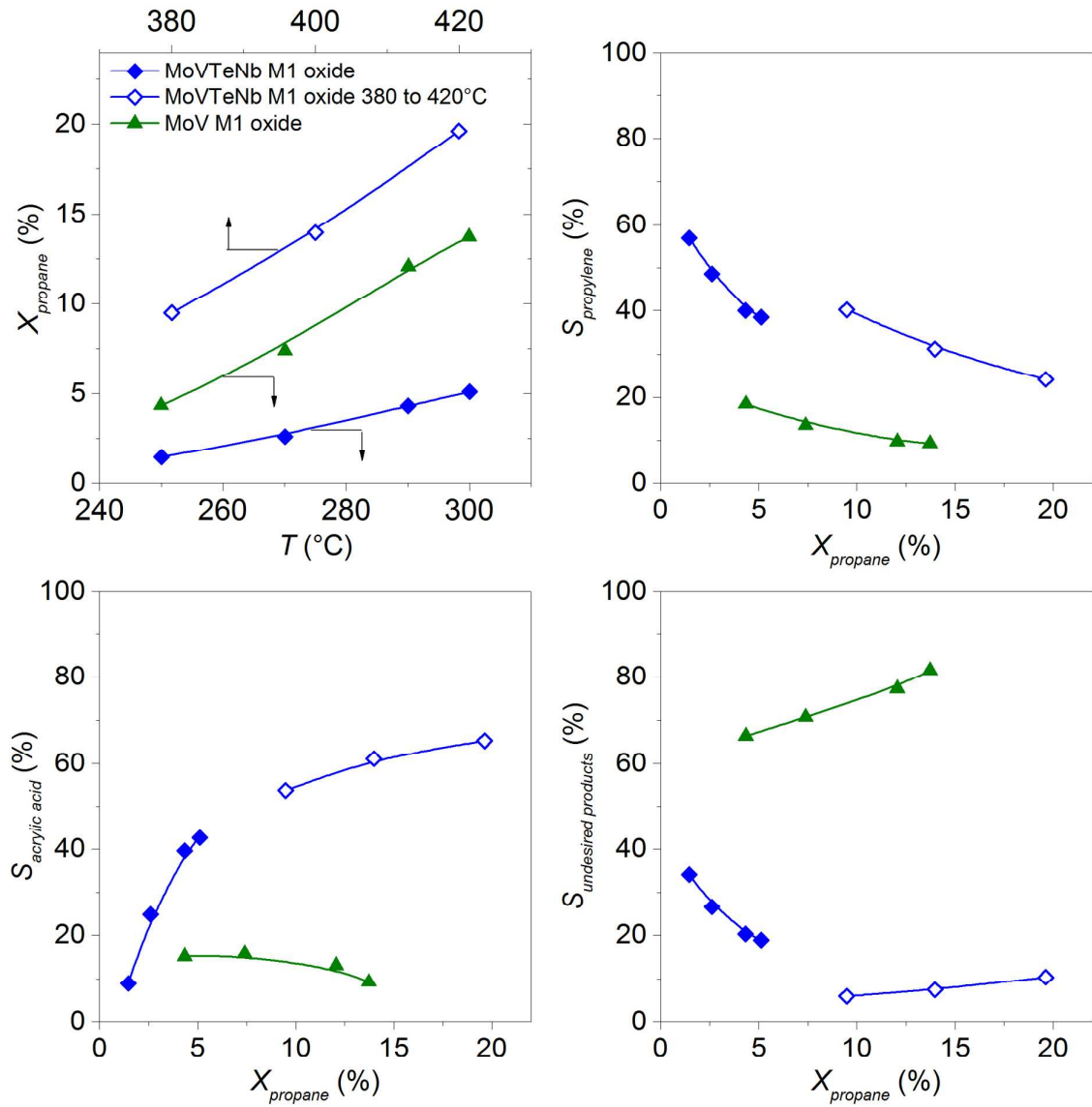


Figure S7. Comparison of MoV and MoVTeNb M1 oxides (full symbols) in the oxidation of propane at $T=250-300^\circ\text{C}$ (feed composition $\text{C}_3/\text{O}_2/\text{N}_2/\text{H}_2\text{O}=3/6/71/20$, $\text{W/F}=0.36 \text{ gsml}^{-1}$); The selectivity as a function of conversion is additionally shown for MoVTeNb M1 oxide at $380-420^\circ\text{C}$ (open symbols) (feed composition $\text{C}_3/\text{O}_2/\text{H}_2\text{O}/\text{N}_2=3/6/20/71$, $\text{W/F}=0.09 \text{ gsml}^{-1}$).

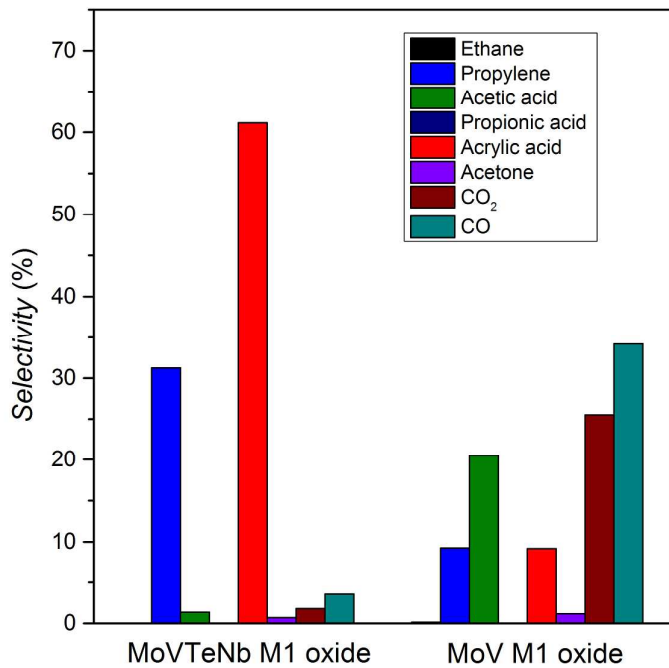


Figure S8. Selectivity in the oxidation of propane at approximately 5 % conversion of propane (feed composition C₃/O₂/N₂/H₂O=3/6/71/20, W/F=0.36 gsm⁻¹) over MoVTeNb (T=290°C) and MoV M1 (250°C) oxides.

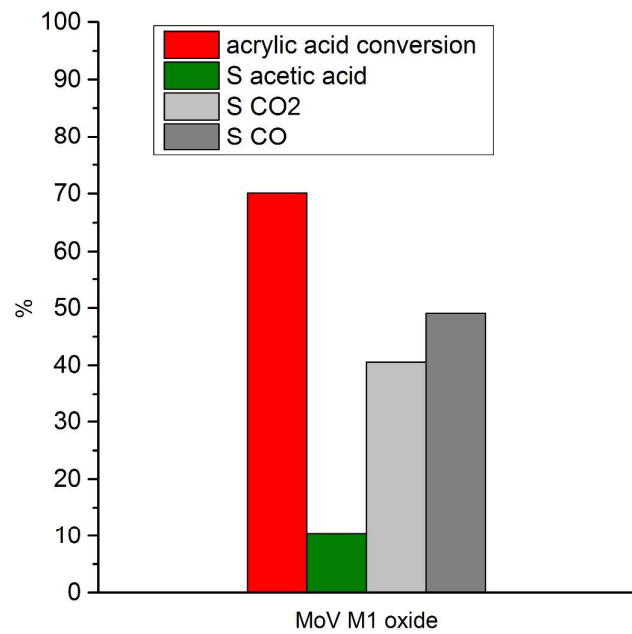


Figure S9. Acrylic acid conversion and product distribution in a feed composed of 0.08 vol% acrylic acid, 2.8 vol% oxygen, and 96.4 vol% He passed over MoV M1 oxide ($m = 85$ mg) at T=300°C. A feed of 5 ml/min synthetic air was saturated at 20°C with acrylic acid and mixed with 20 ml/min He.

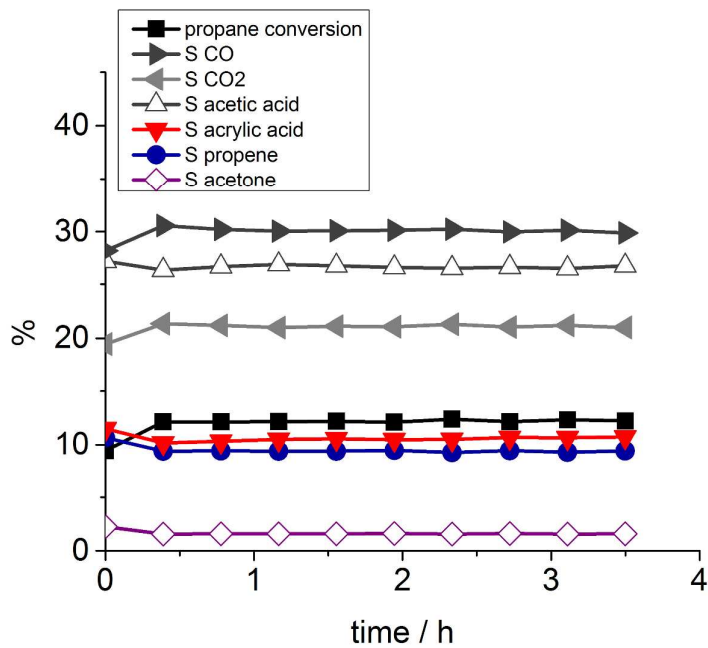


Figure S10. Conversion and selectivity in the oxidation of propane over MoV M1 oxide at T=300°C as a function of time on stream (feed composition C₃/O₂/N₂/H₂O=3/6/51/40, W/F=0.36 gsm⁻¹).

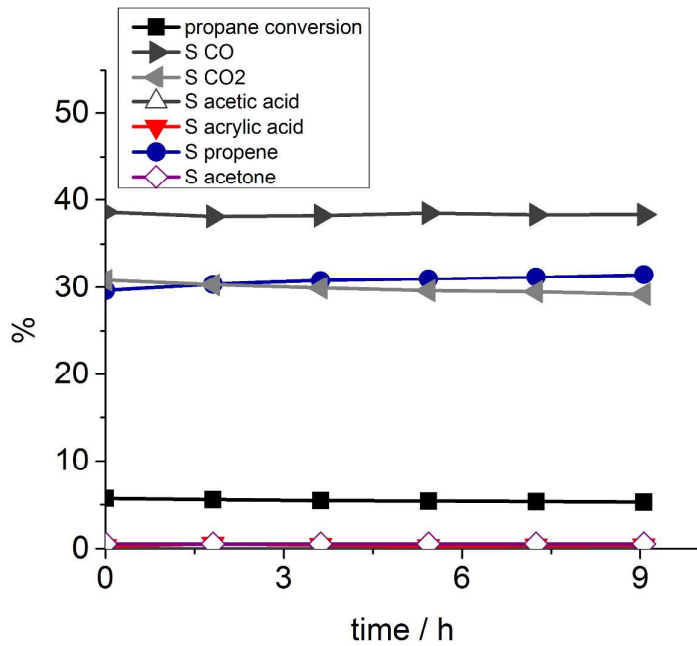


Figure S11. Conversion and selectivity in the oxidation of propane over MoV M1 oxide at T=300°C as a function of time on stream (feed composition C₃/O₂/N₂/H₂O=3/6/91/0, W/F=0.36 gsm⁻¹).

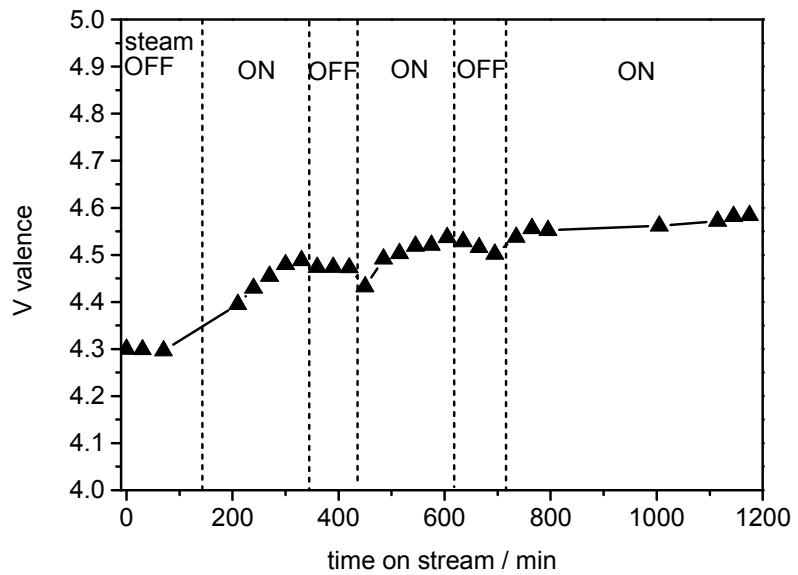


Figure S12. Average valence of vanadium at the surface of $(\text{Mo},\text{V})\text{O}_x$ in the measurement shown in Fig. 6 in the main text.